Giant Goos-Hänchen Effect and Fano Resonance at Photonic Crystal Surfaces

I. V. Soboleva,* V. V. Moskalenko, and A. A. Fedyanin†

Faculty of Physics, Lomonosov Moscow State University, Moscow 119991, Russia

(Received 18 August 2011; published 21 March 2012)

The Goos-Hänchen effect and Fano resonance are studied in photonic crystals that are considered Fourier counterparts in wave-vector-coordinate space. The Goos-Hänchen effect, which is enhanced by the excitation of Bloch surface electromagnetic waves, is visualized using far-field microscopy and measured at the surface of photonic crystals by angular spectroscopy. The maximal Goos-Hänchen shift is observed to be 66 μm.

DOI: 10.1103/PhysRevLett.108.123901 PACS numbers: 42.70.Qs, 78.67.Pt

The spatial displacement of a beam totally reflected from a dielectric surface, which is predicted by Newton's corpuscular theory of optics, was first observed by Goos and Hänchen in 1947 [1]. Since then, the Goos-Hänchen (GH) effect has been extended to many fields of physics, including acoustics [2], quantum mechanics [3–5], radiophysics [6], and nonlinear optics [7]. The effect has been the subject of intensive theoretical [8–10] and experimental research [11–14]. Several models have been developed to interpret the appearance of the GH effect, including stationary phase [15,16] and energy propagation [17] approximations. Artmann [15] proposed the following relation between the Goos-Hänchen shift (GHS) D and the change in the complex reflection coefficient phase:

$$D = -\frac{\lambda}{2\pi}\frac{\partial\varphi(\theta)}{\partial\theta}, \tag{1}$$

where λ is the wavelength, $\varphi(\theta)$ is the phase of the reflection coefficient r, and θ is the angle of incidence at the interface. It has been subsequently shown that for reflectance angular resonances with a small derivative of the phase (for example, in the vicinity of the angle of total internal reflection [18], near the (pseudo-) Brewster-effect angle [19], or at the edge of the photonic band gap [20]), the GHS does not exceed 10 times the incident light wavelength. A narrower resonance in the angular reflectance spectrum is required to increase the GHS value (for example, through the excitation of surface states). Recently, a significant enhancement of the GH effect was achieved by the excitation of plasmons on metal surfaces [21,22] and Bloch surface electromagnetic waves (SEWs) in photonic crystals [23].

Discrete surface states often lead to the appearance of an asymmetric Fano-shape resonance in the reflectance spectra. Fano resonance is caused by the interaction of a spectrally narrow discrete state with a continuous spectrum. It is found in a wide range of phenomena, such as autoionization in atoms [24], quantum dot conductivity [25], and the transmittance of electron-phonon systems [26] and semiconductor superlattices [27]. The first model describing the asymmetric spectrum was used to interpret the autoionization spectra of He atoms [24]. As a result, the factor F, which describes the Fano-shaped resonance in a spectrum of energy $\mathcal{E}$, was expressed in the following form:

$$F = \frac{(q+\epsilon)^2}{1+\epsilon^2}, \qquad \epsilon = \frac{\mathcal{E}-\mathcal{E}_{\mathrm{res}}}{\frac{1}{2}\Gamma}, \tag{2}$$

where q is the Fano constant, $\mathcal{E}_{\mathrm{res}}$ is the energy of the resonance, and Γ is the resonance spectral width. Fano resonance is now widely studied in various optical systems, including metamaterials [28], plasmon-active nanostructures with extraordinary optical transmission [29], photonic crystals [30], and microcavities [31,32].

Both the Fano resonance and the Goos-Hänchen effects can be observed simultaneously through the excitation of optical surface states because they are both caused by changes in the phase of the complex reflection coefficient. The phase change leads to beam interference causing Fano resonance in the reflectance spectra and the simultaneous lateral shift of the reflected beam resulting in the GH effect. The Fano resonance and the GH effect are indirectly related, as they are measures of the SEW mean free path and the energy transfer resulting from the SEW, respectively.

In this Letter, Fano resonance and the Goos-Hänchen effect caused by Bloch surface waves excited in photonic crystals are studied. They are treated as manifestations of the same phenomenon in the Fourier-conjugated wave vector and coordinate domains. Using the same set of adjustable parameters, both effects are described in terms of the change in the reflection coefficient phase.

Fano resonance behavior and the enhancement of the GH effect are studied in the case of SEWs at one-dimensional (1D) photonic crystal surfaces [33]. An extremely narrow SEW angular resonance leads to appreciable GHS enhancement [23], making SEWs a convenient tool for the study of the GH effect. Multilayer structures consisting of 9, 11, 13, and 15 ZrO_2/SiO_2 bilayers with refractive indices of 1.9 and 1.46 were chosen as 1D photonic crystal samples (i.e., distributed Bragg reflectors). The bilayers were deposited on cover glasses with a refractive index of 1.51. The period of the photonic crystals

in the series was fixed to 250 ± 10 nm, which was determined by scanning electron microscopy of the sample edge as shown in Fig. 1(a). An attenuated total internal reflection prism configuration, shown in Fig. 1(b), was used to couple the incident *s*-polarized light to the SEW at the photonic crystal–air interface because *p*-polarized light did not excite the SEW in the studied samples. Contact between the sample (S) and the hemicylinder (H) was made with a layer of index-matching liquid (an aqueous solution of glycerol). A cw single-mode laser (L) operating at $\lambda = 532$ nm, with power less than 10 mW and an angular divergence of 2.5 mrad, was used as a light source. The hemicylinder was placed on a rotation stage for the fine control of the angle of incidence θ. The reflected light intensity was detected by a photodiode (PD). Note that visualization of the evanescent surface waves at the smooth surface in the far field is impossible. However, the rescattering of SEWs across surface microroughness enables their observation in the far field, which is a technique used to visualize surface plasmons [34]. The same approach was applied in this study for the visualization of SEWs in the far field by optical microscopy [35]. An objective lens (O) with a numerical aperture of 0.28 was focused at the surface of the photonic crystal (S) to collect the SEW scattered radiation. The image was then detected by a CCD camera. A typical plot of reflectance R as a function of the incident angle θ is shown in Fig. 1(c). At a specific incident angle above the critical angle, the evanescent field penetrates through the multilayer and excites the SEW at the photonic crystal–air interface. This leads to a narrow reflectance dip. Figure 1(d) shows a typical microimage of the SEW excited at the surface of the photonic crystal. The SEW is spatially distributed in a cometlike pattern stretched along the propagation direction, with the intensity profile shown in Fig. 1(e). The SEW mean free path is estimated as 115 μm. Direct GHS visualization was performed using a new approach based on the local fluorescence detection shown in Fig. 1. Contact between the photonic crystal substrate (S) and the BK7 right-angle prism (P) was made using an index-matching liquid (I), which was an ethanol solution of Rhodamine 6 G ($10^{-5}M$) mixed with an aqueous solution of glycerol in a 1:100 ratio. The incident and reflected beams passing through the index-matching liquid were visualized by detection of spots of dye fluorescence, "*inc*" and "*ref*," respectively. An orange filter (F) was placed behind the objective lens (O) in front of the CCD camera8 as a pump radiation cutoff. The deviation in distance between *inc* and *ref* caused by different thicknesses of photonic crystal samples is approximately 2% and lies within measuring inaccuracy. The GHS value was determined by comparing the position of *ref* spots for *p*- (without SEW) and *s*-polarized (with SEW) beams.

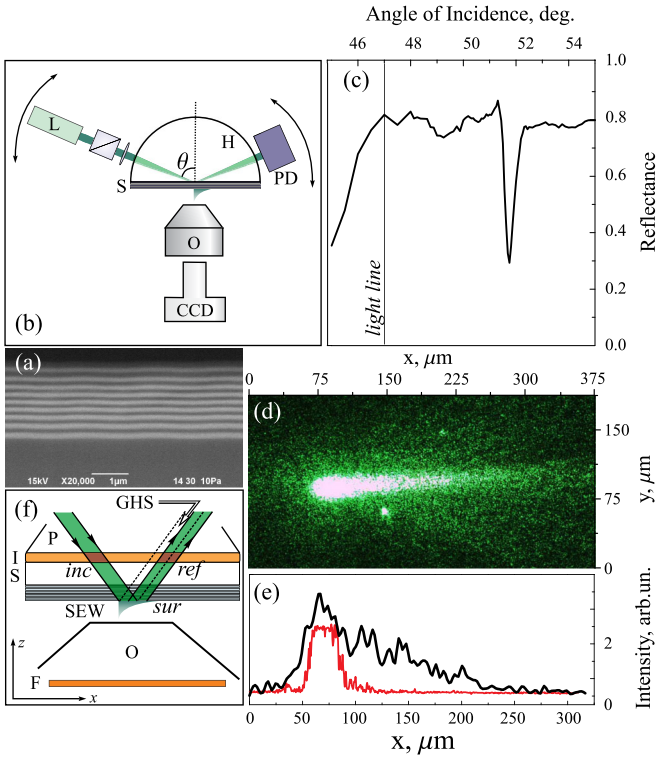

FIG. 1 (color online). (a) Typical SEM image of the 1D photonic crystal edge. (b) Schematic of the experimental setup for reflectance angular spectroscopy and microscopy. (c) Typical reflectance angular spectrum of a 1D photonic crystal with 15 bilayers obtained in the Kretschmann configuration for *s*-polarized incident light. The *light line* marks the angle of total internal reflection. The dip at 52° indicates SEW resonance. (d) Microimage of a SEW at the 1D photonic crystal surface. (e) Profiles of intensity distribution at the photonic crystal surface for the *s* (black line) and *p* (red line) polarizations of the incident light. (f) Sketch of the GHS observation scheme via dye fluorescence.

A typical angular reflectance spectrum of a photonic crystal in the Kretschmann configuration, which is modeled for a fixed wavelength using the transfer matrix technique [36,37], is shown in Fig. 2(a). The narrow dip at $\theta_{\mathrm{SEW}} \simeq 51°$ corresponds to the SEW resonance, while the wide dip at lower angles is caused by the excitation of the guided mode inside the photonic crystal [33]. The experimental angular reflectance spectra of the photonic crystals are shown in Figs. 2(b)–2(e). The spectral features in the vicinity of $\theta_{\mathrm{SEW}} \simeq 51°$ are related to the SEW resonance at the 1D photonic crystal surface. SEW sensitivity to the structure of the photonic crystal, especially to the thickness of the surface layer, leads to a slight difference in θ_{SEW} from one sample to another. The asymmetric line shape is associated with Fano-type resonance that is caused by the partial transfer of incident light energy to the SEW due to the extremal narrowness of the SEW resonance. The incident-beam angular divergence is larger than the angular width of the resonance, leading the beam to split into two components: the component resonantly transferred to the SEW and partly reemitted back into the prism, on the one hand, and the component totally reflected from the

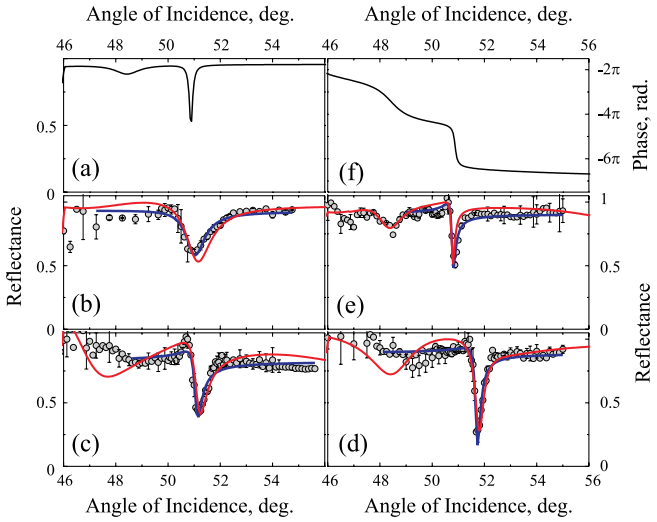

FIG. 2 (color online). (a) The model angular reflectance spectrum of the 1D photonic crystal below the light line. (b)–(e) Experimental angular reflectance spectra (circles) of samples with 9, 11, 13, and 15 bilayers, respectively, and their fits according to Eq. (2) (blue [dark gray] curves) and Eq. (3) (red [medium gray] curves). Incident light is s polarized. Dips in the spectra correspond to SEW excitation. (f) The model angular spectrum of the phase of the complex reflection coefficient.

surface of the photonic crystal, on the other. Interference of these two components results in Fano resonance in the reflectance spectrum. The experimental spectra are fitted by Fano resonance in the form Eq. (2) with $\epsilon = (k - k_{\mathrm{res}})/\Gamma$, where $k = 2\pi n \sin\theta/\lambda$ is the tangential component of the wave vector of the incident light, k_{res} is the SEW wave-vector module, and n is the refractive index of the photonic crystal top layer. The SEW mean free path L is obtained based on a resonance width Γ as $L = 2\pi/\Gamma$. The value of L increases with an increase in the photonic crystal thickness; it is equal to 24, 65, 90, and 130 μm for samples with 9, 11, 13, and 15 bilayers, respectively. These data, which were extracted from the reflectance spectra, are also supported by the SEW microscopic images, which is shown for the 15-bilayer photonic crystal in Figs. 1(d) and 1(e).

The Fano profile given by Eq. (2) cannot provide the relative phase φ of the complex reflection coefficient r. Therefore, GHS, which is governed by the phase derivative in Eq. (1), cannot be extracted directly from the angular reflectance spectra. However, fitting the experimental dependences with the square of the reflection coefficient module calculated by the transfer matrix method allows one to obtain the angular dependences of the complex reflection coefficient, from which the phase of the reflection coefficient can be extracted.

Let us denote the complex amplitude of the electromagnetic field component resonantly transferred into the SEW by E_r^{res}, while the complex amplitude of the component totally reflected from the photonic crystal surface is denoted by E_r^{unres}. These amplitudes are added together and weighted by the coefficient a. The a parameter is similar to the Fano parameter q in Eq. (2), as it is a part of the light energy transferred into the resonant state. Reflectance R is given as follows:

$$R \equiv |r|^2 = \left| \frac{E_r^{\mathrm{res}} + aE_r^{\mathrm{unres}}}{E_i} \right|^2, \tag{3}$$

where E_i is the amplitude of the incident electromagnetic field. In terms of fit, the Eq. (3) [see Figs. 2(b) and 2(e)] shows good agreement with the experimental data in the angular vicinity of the SEW resonance. The angular dependence of the reflection coefficient phase, $\varphi(\theta)$, can be calculated. Figure 2(f) shows the typical dependence $\varphi(\theta)$, which is calculated from the fit of the experimental angular spectra $R(\theta)$. The dependence exhibits a step at $\theta \simeq 51°$ that corresponds to a SEW-induced phase drop determined by the depth and narrowness of the reflectance resonance. Thus the significant GHS enhancement is expected to be observed in the vicinity of the SEW resonance. The GHS estimation by using Eq. (1) gives the realistic values if the incident-beam spatial spectrum is narrow enough. In the general case the position of reflected field $E_r(x)$ can be found as follows:

$$E_r(x) = \frac{1}{2\pi} \int_{-\infty}^{\infty} r(k_x)\bar{E}_i(k_x)e^{\imath k_x x} dk_x, \tag{4}$$

where $\bar{E}_i(k_x)$ is the Fourier spectrum of the incident beam (e.g., see [28]). See the Supplemental Material [38] for detailed calculations.

A direct visualization of the GH effect at the surfaces of the photonic crystals is presented in Fig. 3. The microimages obtained from a microscope focused on the photonic crystal surface is shown in Figs. 3(a) and 3(b). The bright spot, *sur*, in the center of Fig. 3(b) is related to the total internal reflection of p-polarized beam at the surface of the sample. The cometlike shape spot *sur* in Fig. 3(a) is associated to SEW scattering. Two orange spots, *inc* and *ref*, respectively, correspond to the fluorescent spots induced by the incident and the reflected beams passing through the Rhodamine-doped immersion liquid. The position of the reflected spot is shifted for the incident s-polarized light undergoing the GHS due to SEW excitation at the surface of photonic crystal. The GHS was observed by focusing the objective lens in the index-matching layer and cutoff the green laser radiation. Figures 3(d)–3(g) show the *ref* cross sections of the s-polarized reflected beam in photonic crystals of different thicknesses. For comparison, a microimage of the *ref* spot of the p-polarized beam is shown in Fig. 3(c).

The reflected spot consists of two parts. One part of the beam is spatially fixed and relates to the nonresonant part of the incident light totally reflected from the photonic crystal surface. The shifting part of the beam corresponds

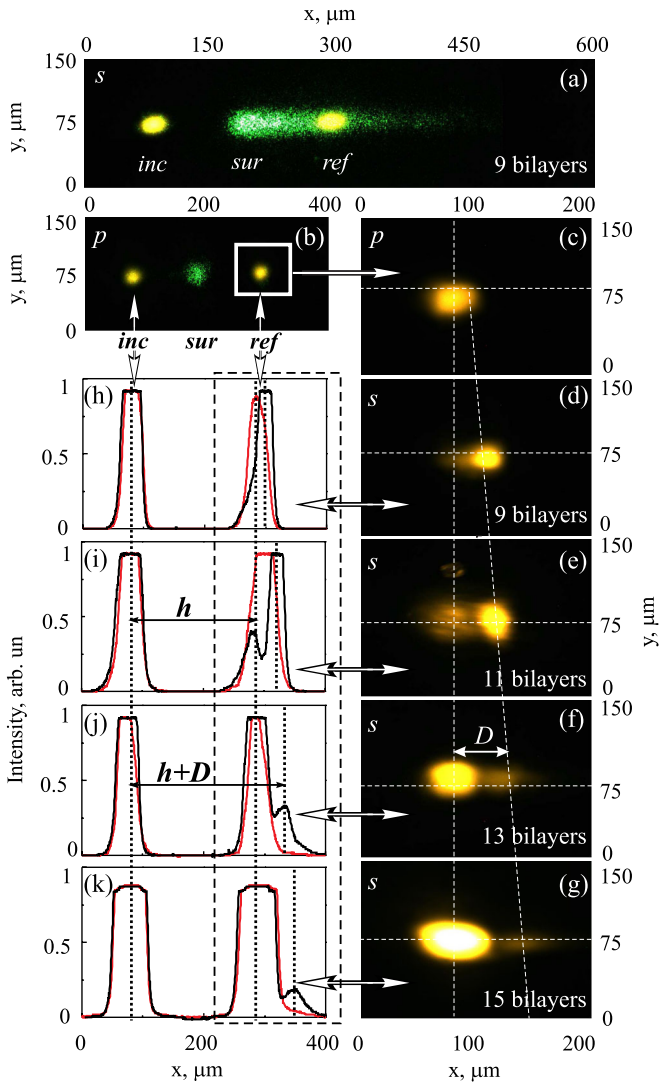

FIG. 3 (color online). Microimages of the surface of the photonic crystal illuminated with *s*- (a) and *p*-polarized (b) light. The objective lens is focused on the photonic crystal surface. (c) Fluorescence microimage of the reflected *p*-polarized beam. The objective is focused in the immersion liquid layer. (d)–(g) Fluorescence microimages of the *s*-polarized beam reflected from photonic crystals with different numbers of bilayers. The GHS is marked as *D*. (h)–(k) Fluorescence intensity profiles of *s*- (black line) and *p*-polarized (red line) beams. Left and right peaks corresponds to *inc* and *ref* spots.

to the light resonantly coupled into the SEW and reemitted back into the prism. The GHSs are obtained from the distributions of the fluorescence intensities shown in Figs. 3(h)–3(k). Distance between *inc* and *ref* spots in case of *p*-polarized light, *h*, corresponds to the projection of the beam optical path to the objective focal plane. Since the incidence of the *p*-polarized light cannot lead to SEW-enhanced GHS, the distance between the shifted maximum of the *s*-polarized reflected beam and the nonshifted *p*-polarized reflected beam reveals the absolute GHS value, *D*.

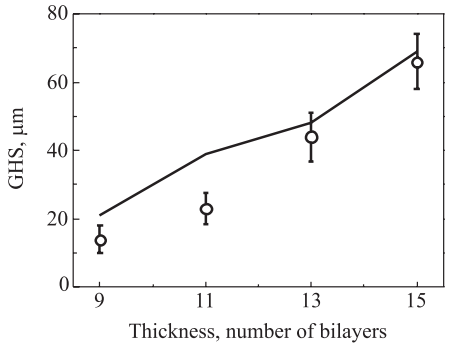

FIG. 4. The GHSs at the SEW resonances, which are measured (circles) and fitted from Fano-shaped reflectance spectra with Eq. (4) (line) in dependence on the number of bilayers in the photonic crystal.

Figure 4 shows the GHS as a function of the number of bilayers in the photonic crystal, measured from fluorescence intensity profiles shown in Figs. 3(h)–3(k). The line shows the GHS values in the SEW resonance obtained from the Fano-shaped reflectance spectra fitted by the transfer matrix method shown in Figs. 2(b)–2(e). The GHS increases with an increase of the photonic crystal thickness. The largest GHS is equal to 66 μm and is observed in the photonic crystal with 15 bilayers, which is in agreement with the data obtained from the fits to the angular reflectance spectra within the experimental error bars.

In conclusion, the simultaneous analysis of the Goos-Hänchen effect and Fano resonances in 1D photonic crystals, which was performed by angular spectroscopy and far-field microscopy, reveals their dependence on the photonic crystal thickness. The Goos-Hänchen effect is directly visualized at the surface of the photonic crystals using far-field microscopy; it is also extracted from an approximation of the reflectance angular spectra with Fano-profile resonances. The maximal value of the observed Goos-Hänchen shift is 66 μm (125λ), which is at least 1 order of magnitude larger than the value at the dielectric surface. Such a large GHS and the proposed method of GHS analysis can improve the functionality of sensors composed of photonic crystals and may have an impact on the further development of sensor technology.

We are grateful to E. Descrovi for stimulating discussions. This work was supported by the Russian Foundation of Basic Research and the Russian Ministry of Education and Science.

*Also at: A. N. Frumkin Institute of Physical Chemistry and Electrochemistry, Russian Academy of Science, Moscow 119991, Russia.
†fedyanin@nanolab.phys.msu.ru

[1] F. Goos, H. Hänchen, Ann. Phys. (Leipzig) **436**, 333 (1947).

[2] R. Briers, O. Leroy, and G. Shkerdin, J. Acoust. Soc. Am. **108**, 1622 (2000).
[3] V. K. Ignatovich, Phys. Lett. A **322**, 36 (2004).
[4] V.-O. de Haan, J. Plomp, T. M. Rekveldt, W. H. Kraan, A. A. van Well, R. M. Dalgliesh, and S. Langridge, Phys. Rev. Lett. **104**, 010401 (2010).
[5] H. Hora, Optik (Stuttgart) **17**, 409 (1960).
[6] A. Matthews and Yu. Kivshar, Appl. Phys. Lett. **93**, 131901 (2008).
[7] O. Emile, T. Galstyan, A. Le Floch, and F. Bretenaker, Phys. Rev. Lett. **75**, 1511 (1995).
[8] C. K. Carniglia and K. R. Brownstein, J. Opt. Soc. Am. **67**, 121 (1977).
[9] B. R. Horowitz and T. Tamir, J. Opt. Soc. Am. **61**, 586 (1971).
[10] T. Paul, C. Rockstuhl, C. Menzel, and F. Lederer, Phys. Rev. A **77**, 053802 (2008).
[11] M. Merano, J. B. Götte, A. Aiello, M. P. van Exter, and J. P. Woerdman, Opt. Express **17**, 10864 (2009).
[12] Yu. Wan, Zh. Zheng, and J. Zhu, J. Opt. Soc. Am. B **28**, 314 (2011).
[13] F. Bretenaker, A. Le Floch, and L. Dutriaux, Phys. Rev. Lett. **68**, 931 (1992).
[14] W. Löffler, M. P. van Exter, G. W. 't Hooft, E. R. Eliel, K. Hermans, D. J. Broer, and J. P. Woerdman, Opt. Commun. **283**, 3367 (2010).
[15] K. Artmann, Ann. Phys. (Leipzig) **437**, 87 (1948).
[16] K. W. Chiu and J. J. Quinn, Am. J. Phys. **40**, 1847 (1972).
[17] R. H. Renard, J. Opt. Soc. Am. **54**, 1190 (1964).
[18] H. G. L. Schwefel, W. Köhler, Z. H. Lu, J. Fan, and L. J. Wang, Opt. Lett. **33**, 794 (2008).
[19] M. Merano, A. Aiello, G. W. t' Hooft, M. P. van Exter, E. R. Eliel, and J. P. Woerdman, Opt. Express **15**, 15928 (2007).
[20] D. Felbacq, Opt. Lett. **28**, 1633 (2003).
[21] C. Bonnet, D. Chauvat, O. Emile, F. Bretenaker, and A. Le Floch, Opt. Lett. **26**, 666 (2001).
[22] X. Yin, L. Hesselink, Z. Liu, N. Fang, and X. Zhang, Appl. Phys. Lett. **85**, 372 (2004).
[23] V. V. Moskalenko, I. V. Soboleva, and A. A. Fedyanin, JETP Lett. **91**, 382 (2010).
[24] U. Fano, Phys. Rev. **124**, 1866 (1961).
[25] A. A. Clerk, X. Waintal, and P. W. Brouwer, Phys. Rev. Lett. **86**, 4636 (2001).
[26] L. A. Fal'kovskii, JETP Lett. **62**, 242 (1995).
[27] C. P. Holfeld, F. Löser, M. Sudzius, K. Leo, D. M. Whittaker, and K. Köhler, Phys. Rev. Lett. **81**, 874 (1998).
[28] I. V. Shadrivov, A. A. Zharov, and Yu. S. Kivshar, Appl. Phys. Lett. **83**, 2713 (2003).
[29] M. R. Shcherbakov, M. I. Dobynde, T. V. Dolgova, D.-P. Tsai, and A. A. Fedyanin, Phys. Rev. B **82**, 193402 (2010).
[30] M. V. Rybin, A. B. Khanikaev, M. Inoue, K. B. Samusev, M. J. Steel, G. Yushin, and M. F. Limonov, Phys. Rev. Lett. **103**, 023901 (2009).
[31] M. Galli, S. L. Portalupi, M. Belotti, L. C. Andreani, L. O'Faolain, and T. F. Krauss, Appl. Phys. Lett. **94**, 071101 (2009).
[32] R. Harbens, S. Jochim, N. Moll, R. F. Mahrt, D. Erni, J. A. Hoffnagle, and W. D. Hinsberg, Appl. Phys. Lett. **90**, 201105 (2007).
[33] W. M. Robertson and M. S. May, Appl. Phys. Lett. **74**, 1800 (1999).
[34] H. Raether, *Surface-Plasmons on Smooth and Rough Surfaces and on Gratings* (Springer Tracts in Modern Physics, Berlin, 1988).
[35] I. V. Soboleva, E. Descrovi, C. Summonte, A. A. Fedyanin, and F. Giorgis, Appl. Phys. Lett. **94**, 231122 (2009).
[36] D. S. Bethune, J. Opt. Soc. Am. **6**, 910 (1989).
[37] *Handbook of Optical Constants of Solids*, edited by E. D. Palik (Academic, New York, 1985).
[38] See Supplemental Material at http://link.aps.org/supplemental/10.1103/PhysRevLett.108.123901 for details of calculations of GHS using the Fourier spectrum of the incident beam.